Low Froude Number Flow Past Three-Dimensional Obstacles. Part I: Baroclinically Generated Lee Vortices

PIOTR K. SMOLARKIEWICZ AND RICHARD ROTUNNO

National Center for Atmospheric Research, Boulder, Colorado*

(Manuscript received 6 May 1988, in final form 14 October 1988)

ABSTRACT

We study the flow of a density-stratified fluid past a three-dimensional obstacle, using a numerical model. Our special concern is the response of the fluid when the Froude number is near or less than unity. Linear theory is inapplicable in this range of Froude number, and the present numerical solutions show the rich variety of phenomena that emerge in this essentially nonlinear flow regime. Two such phenomena, which occupy Parts I and II of this study, are the formation of a pair of vertically oriented vortices on the lee side and a zone of flow reversal on the windward side of the obstacle. The lee vortices have been explained as a consequence of the separation of the viscous boundary layer from the obstacle; however, this boundary layer is absent (by design) in the present experiments and lee vortices still occur. We argue that a vertical component of vorticity develops on the lee side owing to the tilting of horizontally oriented vorticity produced baroclinically as the isentropes deform in response to the flow over the obstacle. This deformation is adequately predicted by linear gravity-wave theory, which allows one to deduce, using the next-order correction to linear theory, the existence of a vortex pair of the proper sense in the lee of the obstacle. Thus, the lee vortices are closely associated with the dynamics of gravity waves. The generation of the lee vortices may also be understood as a consequence of Ertel's theorem which in the present circumstance demands that vortex lines adhere to isentropic surfaces—since the isentropes are depressed behind the hill, the vortex lines must run upward and downward along the depression implying vertically oriented vorticity.

1. Introduction

The original motivation for this work was the desire to understand why cloud "bands" form persistently windward of the island of Hawaii. Smolarkiewicz et al. (1988) have demonstrated by means of numerical experiments and field observations that these cloud bands may be understood in terms of the effectively inviscid response of a density-stratified fluid flowing past a three-dimensional obstacle at low Froude number. (The Froude number, $\mathrm{Fr} \equiv U/Nh$, where U is the flow speed, h is the height of the obstacle, and N, the Brunt–Väisällä frequency, is a measure of the stratification; in the Hawaiian situation, $\mathrm{Fr} \sim 0.1$–0.4.) In particular, it was shown that on the windward side a zone of flow reversal forms at low Fr; associated with this zone is the convergence they believe to be primarily responsible for Hawaii's windward cloud band. The other salient feature that appeared in their numerical experiments was intense vertically oriented vortices on the lee side of the island, also at low Fr. In Part I of this study we investigate the mechanics of the lee vortices through idealized numerical experiments and analytical theory; in Part II we will, by similar means, concentrate on the windward flow-reversal zone.

Although the computations alluded to above were effectively inviscid, and for a low-aspect-ratio (height/length ~ 0.05) obstacle, a number of features typically observed in several moderate-Reynolds-number, aspect-ratio-unity laboratory flows (Brighton 1978; Hunt and Snyder 1980; Castro et al. 1983; Snyder et al. 1985) were obtained. In the laboratory studies, the lee vortices have been attributed to the separation of the viscous boundary layer from the lower surface. However, in the numerical experiments there was (by design) no viscous boundary layer because a "zero-stress" (or "free-slip") boundary condition was applied on the lower surface and lee vortices still formed. It was for this reason Smolarkiewicz et al. (1988) conjectured that the lee vortices observed in stratified-flow laboratory experiments and in relevant atmospheric flows could be generated by a purely inviscid process.

The existence of a lee vortex implies vertically oriented vortex lines in the vicinity of the vortex center. In the idealized calculations reported on herein there is no vertically oriented vorticity (hereinafter, simply "vertical vorticity") in the base state and no direct generation of vertical vorticity at the side walls of the obstacle in consequence of the zero-stress conditions

* The National Center for Atmospheric Research is sponsored by the National Science Foundation.

Corresponding author address: Dr. Piotr K. Smolarkiewicz, NCAR/MMM, P.O. Box 3000, Boulder, CO 80307-3000.

there. Hence the lee vortices that develop must acquire their vertical vorticity through the tilting of horizontal vorticity into the vertical. However, the base flow is constant over space and so possesses zero horizontal vorticity. We shall demonstrate that it is the horizontal vorticity generated baroclinically (as the stratified flow passes over the obstacle) and tilted behind the obstacle that accounts for the vertical vorticity of the lee vortices.

The laboratory studies indicate that the upwind flow reversal could be a manifestation of the separation of the windward boundary layer as it experiences the adverse pressure gradient associated with the slowing of the wind upon reaching the obstacle and/or upwind effects such as those known to occur in effectively inviscid, two-dimensional, stratified flow (e.g., Pierrehumbert and Wyman 1985). In the present numerical experiments we eliminate the possibility of the former mechanism since we apply zero-stress conditions at the lower surface; in this manner we can isolate the effectively inviscid aspects of the three-dimensional stratified flow. We find that a stagnation point occurs on the upwind side of the obstacle as Fr passes below that indicated by Smith's (1980) linear calculation for steady, stratified flow over a bell-shaped obstacle; we elaborate on this, and investigate the effects of having the obstacle elongated in the cross-stream direction in Part II.

Stratified flow past an obstacle for Fr $\sim$ 0.1–0.5 is not covered by existing theories. Linear gravity-wave theories (e.g., Crapper 1959; Smith 1980) are formally valid when Fr $\gg$ 1 while potential-flow-type theory (Hawthorne and Martin 1955; Drazin 1961) is valid when Fr $\ll$ 1. Thus, numerical simulation is presently the only way to gain access to the dynamics of the flow in this range of Fr. From the viewpoint of atmospheric applications the range Fr $\sim$ 0.1–0.5 is of special interest: considering typical tropospheric values of $U \approx 10$ m s^{-1} and $N \approx 0.01$ s^{-1} results in Fr $\approx 1/h$ [km]. Thus flow over mountains of height exceeding $\sim$2 km will have Fr < 0.5. Natural flows characterized by Fr < 0.1 will be sensitive to the effects of surface thermal forcing (Smolarkiewicz et al. 1988); these effects render the previously discussed features peculiar to low-Fr stratified flow far less dominant. To isolate the inviscid aspects of the flow as well as to make our results comparable to existing theories, we shall focus herein on nonrotating, effectively inviscid, uniformly stratified flow past simple three-dimensional obstacles. To retain a connection with actual atmospheric flows, we shall limit our study to slender obstacles that are geometrically similar to mesoscale mountains (and in particular, to the island of Hawaii).

In section 2 we present a brief description of the model and the experimental design. In section 3 we discuss an experiment consisting of a series of uniform-flow simulations with Fr varying from 2.2 to 0.055 where, in order to compare our results with those of linear theory (Smith 1980), we use a three-dimensional, bell-shaped mountain. This experiment shows that the lee vortices and the windward stagnation appear as Fr $\searrow$ 0.5 (for $\searrow$ read "passing from above to below"). In section 4 we investigate the dynamics of the lee vortices. Section 5 contains a discussion and summary of our conclusions.

2. Model description and design of the experiment

The numerical model used in this study is that developed by Clark (1977) and Clark and Farley (1984). The model is a finite-difference approximation to the anelastic, nonhydrostatic equations governing atmospheric motion. The model equations are cast in a nonorthogonal, terrain-following system of coordinates. The finite-difference formulation of the momentum equations employs the Arakawa (1966)-Lilly (1965) second-order algorithm and the second-order-accurate, positive-definite advection transport algorithm of Smolarkiewicz (1984) is used for all scalar conservation equations. The resulting algorithm for the evaluation of the entire system of model equations is second-order-accurate in time and space (Smolarkiewicz and Clark 1986). The fully interactive nesting scheme of Clark and Farley (1984) allows for simultaneous integrations of up to three different domains, each with different resolution.

The boundary conditions for the model variables are specified only for the outermost domain. They include free-slip conditions for the velocity components and zero-flux-type conditions on all scalar variables at the upper and lower surfaces of the model. In order to prevent reflection of vertically propagating gravity waves from the model top, Rayleigh damping and Newtonian cooling are employed in the upper portion of the model domain; grid nesting is not used in the damping region. The lateral boundary conditions are approximated by an open-boundary extrapolation scheme.

The philosophy of the present experimental design is to proceed incrementally from the flow regime where linear theory applies toward the nonlinear regime. The measure of the nonlinearity is the Froude number, U/Nh; all experiments reported herein have a uniform upstream flow in the negative x direction and constant N. Smith (1980) gives the linear solution for steady, hydrostatic, stratified flow past a three-dimensional bell-shaped obstacle:

$$z_h(x, y) = h\left[1 + \left(\frac{x - x_0}{L}\right)^2 + \left(\frac{y - y_0}{L}\right)^2\right]^{-3/2}. \quad (1)$$

To facilitate comparison with linear theory we adopt (1) as the obstacle for study. Since we are interested in mesoscale mountains (such as Hawaii), we fix the obstacle height $h = 0.12L$.

The experiments discussed herein are for Froude numbers 2.2, 1.1, 0.66, 0.55, 0.44, 0.33, 0.22, 0.11, and 0.055. The model covers a horizontal domain of

$20L \times 20L$ with a uniform mesh of 50×50 grid points and a depth of $6\frac{2}{3}h$ is covered by 80 equally spaced points ($\Delta z = h/12$). In the experiments with Fr ≤ 0.66 the gravity wave absorber fills the upper half of the domain. In order to accommodate the increased vertical wavelength of the standing mountain wave in the experiments with Fr = 2.2 and Fr = 1.1, we employed an additional, interactively nested, outer model with the same horizontal domain and resolution, but with a depth of $33\frac{1}{3}h$ covered by a vertical grid increment five times larger than in the lower domain. In the latter two experiments the absorbing layer fills the upper half of the outer model. In all experiments the explicit viscosity is set to zero.

Several methods to begin the computations were tested. The initial flow was given either by: 1) approximately two-dimensional, horizontal, potential flow [similar to the primary flow in Drazin's (1961) theory], 2) impulsive startup with absorption of gravity waves throughout the entire domain during three Brunt–Väisällä periods, or 3) the three-dimensional potential-flow solution. We found that the quasi-stationary solutions reached after $T = tU/L \approx 3$ are not sensitive to the startup procedure. After this time the solution contains all the flow features of the solution at much later times. Unless otherwise stated, the solutions will be considered after $T \approx 9$, when the flow is essentially steady.

3. The Froude-number dependence of flow past a three-dimensional, bell-shaped obstacle

a. Comparison with linear theory

The Froude number may be thought of as the ratio of the mean to the perturbation wind speed since the latter $\sim |Nh|$. Therefore requiring small-amplitude perturbations for the validity of linear theory is tantamount to requiring Fr $\gg 1$. The nonlinear two-dimensional theory embodied in Long's equation (Long 1953) requires for validity no flow reversal. Smith (1977) discusses that flow stagnation occurs in those solutions as Fr passes below unity.

Figures 1–3 display the salient features of the steady-state solutions for Fr = 2.2, 0.66, 0.22, 0.055. Figure 1a–d shows the appearance of lee vortices in the surface streamline pattern (projected onto the $x - y$ plane) as Fr decreases. To facilitate comparison with Smith's (1980) calculation we show in Fig. 2a–d the displacement field of the undisturbed isentropic surface at $z/h = \pi$ Fr/4 (except for Fig. 3d where $z/h = 9\pi$ Fr/4). Finally, Fig. 3a–d shows the streamlines in the vertical cross section through the center plane.

The solution shown in Figs. 1a, 2a and 3a compares well with Smith's (1980) linear solutions: the surface streamline pattern and the displacement field are virtually the same as shown in Smith's (1980) Fig. 4 and Fig. 1b, respectively. The vertical cross section in Fig. 3a shows the vertically propagating-wave pattern familiar from two-dimensional linear theory (Queney 1948) as discussed by Smith (1980, see his Fig. 5).

Inference from linear theory at Fr = 0.66 is highly uncertain since the theory predicts isentropes from above the ground to pass below in the lee as Fr $\searrow 2$ (Smith, 1980). Thus linear theory breaks down (locally at least) long before the value Fr = 0.66 is reached; nonetheless, there are some comparisons worth making. The displacement field in Fig. 2b still resembles that shown in Smith's (1980) Fig. 1b in that it exhibits two separate troughs straddling the obstacle on the lee side, although the isentrope has been displaced to the lower surface as indicated by the absence of contour lines. The lateral deflection of surface streamlines on the lee side, shown in Fig. 1b, increased considerably, in qualitative agreement with Eq. (43) of Smith (1980). The trough of the vertically propagating wave in Fig. 3b moves upwind and becomes narrower, indicating the tendency toward collapse of the isentropic surfaces on the lee slopes of the mountain, again in agreement with Smith's (1980) predictions.

When Fr passes below 0.5 (approximately) the surface streamline pattern evinces a pair of vortices downwind and a small region of reversed flow on the upwind side (Fig. 1c; Fr = 0.22). Figure 2c shows that the region within which the isentropes descend to the lower surface has enlarged. Figure 3c indicates that the vertically propagating mountain wave is far weaker, and below the obstacle top on the lee side, there is a recirculating flow associated with the lee vortices. As remarked upon above, linear theory is technically invalid at these low values of Fr; this, notwithstanding, Smith (1980) has shown that the linear three-dimensional calculation of the perturbation velocity in the x direction at the surface implies that stagnation occurs at $x/L = \sqrt{2}/2$ when Fr $= 2/(3\sqrt{3}) \approx 0.4$, values remarkably close to those obtained here. The almost simultaneous appearance of reversed flow on the lee side is beyond any reasonable interpretation from linear theory as its predictions for the flow there are absurd as Fr $\searrow 2$. The most one can say is that linear theory predicts the collapse of the isentropes to the ground as Fr $\searrow 2$ and that we observe this tendency in the nonlinear model; however, nothing particularly dramatic occurs until Fr $\searrow 0.5$.

For Fr = 0.055, the windward flow is nearly horizontal as the displacements are very small (Fig. 2d) and the streamlines in the vertical cross section (Fig. 3d) are nearly flat. The lee vortices are weaker and shallower (Fig. 3d) than they were for Fr = 0.22. On the windward side our analysis indicates that the flow pattern begins to resemble that found by Drazin (1961; we postpone a detailed discussion of his solution to Part II of this paper).

In summary, linear theory well describes the flow when Fr = 2.2 (as expected) and appears to continue to capture many of the features of interest for Fr greater than approximately 0.5 even though it is formally in-

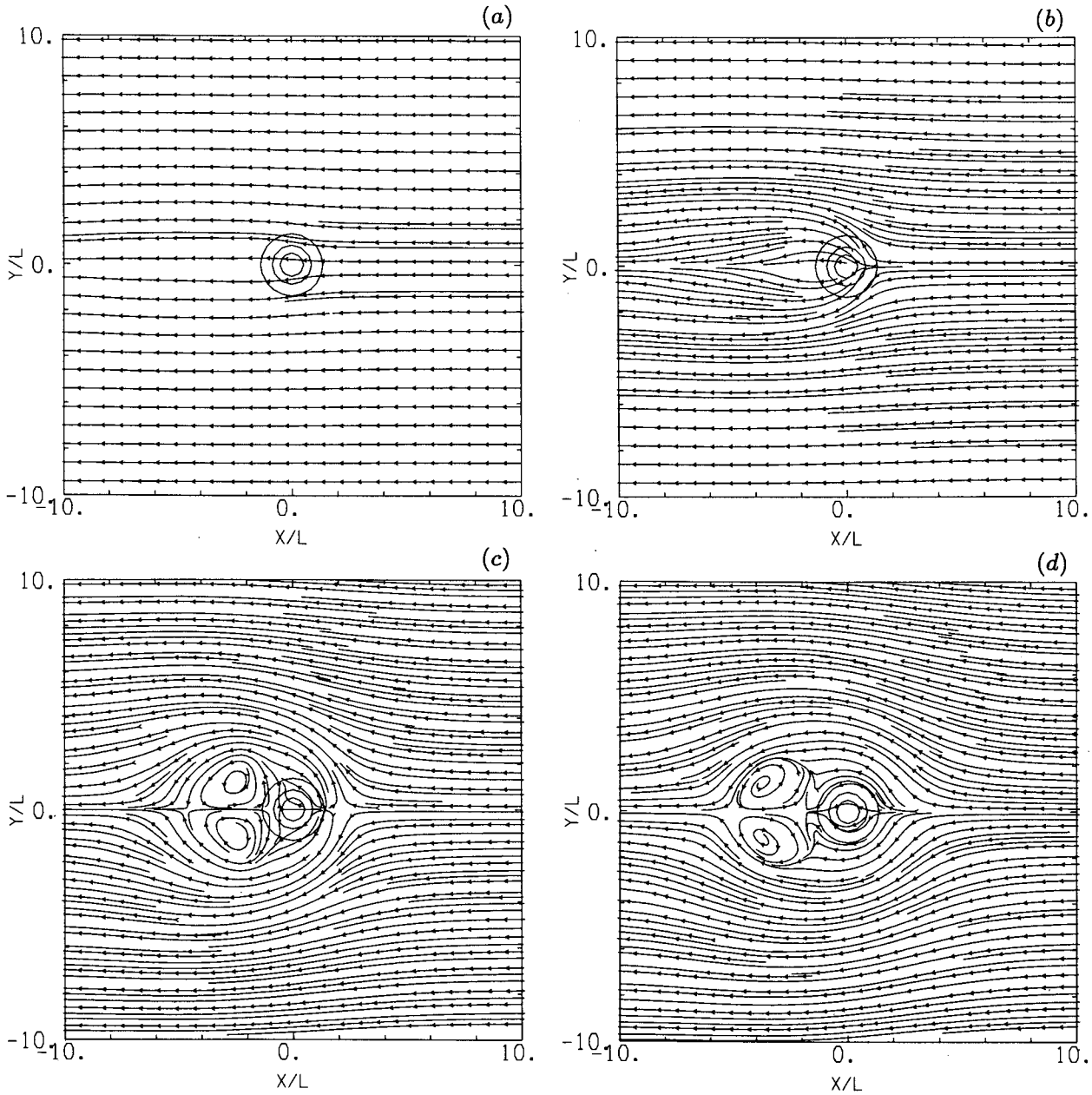

FIG. 1. Steady-state streamlines at the lower surface for Fr = (a) 2.2, (b) 0.66, (c) 0.22, and (d) 0.055. Concentric contours in the center of the domain represent the height of the obstacle with contour interval 0.25 h.

valid in this limit. As Fr $\searrow$ 0.5 flow stagnation occurs on the windward and leeward sides and the flow takes a dramatically different form. Whether or not linear theory describes this flow transition as a function of Fr is not clear. What is clear from these experiments is that the lee vortices and the reversal of the low-level, upwind-side flow seem to appear together as Fr $\searrow$ 0.5 and that the process occurs without viscous-boundary-layer effects. For the remainder of this paper we shall focus on the lee vortices that appear in this low-Fr flow regime.

b. Comparison with laboratory experiments

Although the extant relevant laboratory simulations use obstacles with $h \sim L$, have a no-slip lower surface, and have reflective upper boundary conditions, some of the features are so strikingly similar to the present results that we thought it worthwhile to note them here.

Figure 4 displays a close-up view of the flow on the center plane and surface in the experiment with Fr = 0.22 (Figs. 1c and 3c). This flow is in qualitative agreement with that shown in Fig. 15a of the laboratory

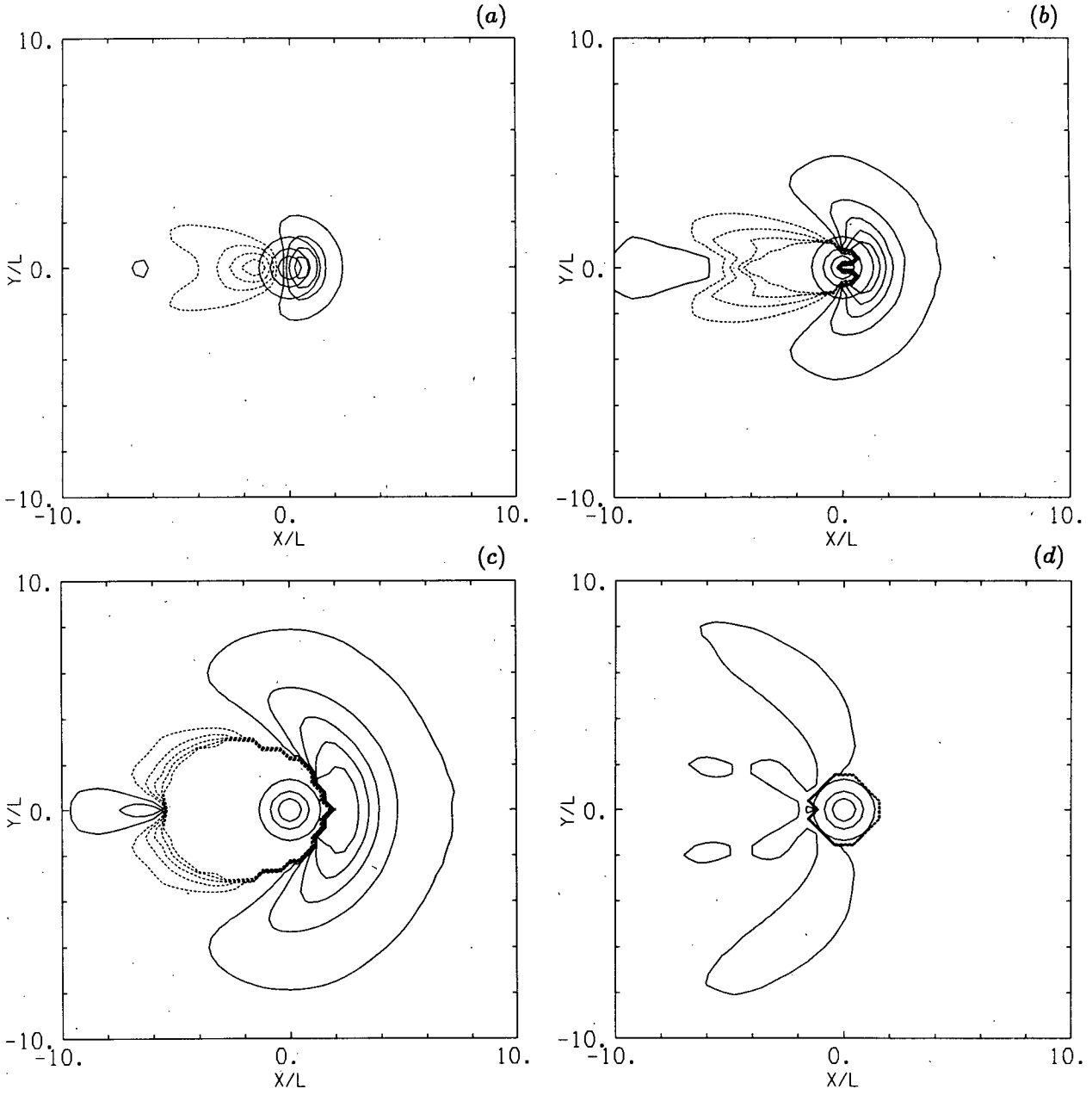

FIG. 2. Displacement field of the isentropic surface with undisturbed height $z/h = \pi\,\mathrm{Fr}/4$ for (a) Fr = 2.2; contour interval, $10^{-4}\,h$, (b) Fr = 0.66; contour interval, $5 \times 10^{-5}\,h$, and (c) Fr = 0.22; contour interval, $1\frac{2}{3} \times 10^{-5}\,h$. In (d) the surface originating at $z/h = 9\pi\,\mathrm{Fr}/8$ is displayed for the experiment with Fr = 0.055; contour interval, $8\frac{1}{3} \times 10^{-6}\,h$. Dashed contour lines indicate negative displacement and zero contour lines are not shown.

study of Hunt and Snyder (1980, hereinafter HS) as the distribution of the singular points of the flow (see also Table 1 of HS) is similar. Progressing in the lower panel of Fig. 4 from right to left along the flow axis, we encounter first the saddle point (P_1 in HS), then further downstream, but still on the windward slope, the nodal point (P_2 in HS). The first singular point on the leeward side is the saddle point (P_3 in HS) below the summit. The centers of the lee vortices represent two nodes (P_4 and $P_4^{(i)}$ in HS). Finally, there is a saddle point downstream of lee vortices on the center axis of flow (P_5 in HS). The upper panel is again similar to the upper panel of HS's Fig. 15a in that the reversed flow in the lee is almost as high as the obstacle and extends leeward a distance of $\sim L$.

Figure 5 summarizes the Fr dependence of certain features of the flow associated with the lee vortices. Figure 5a shows the intensity of the lee vortices as mea-

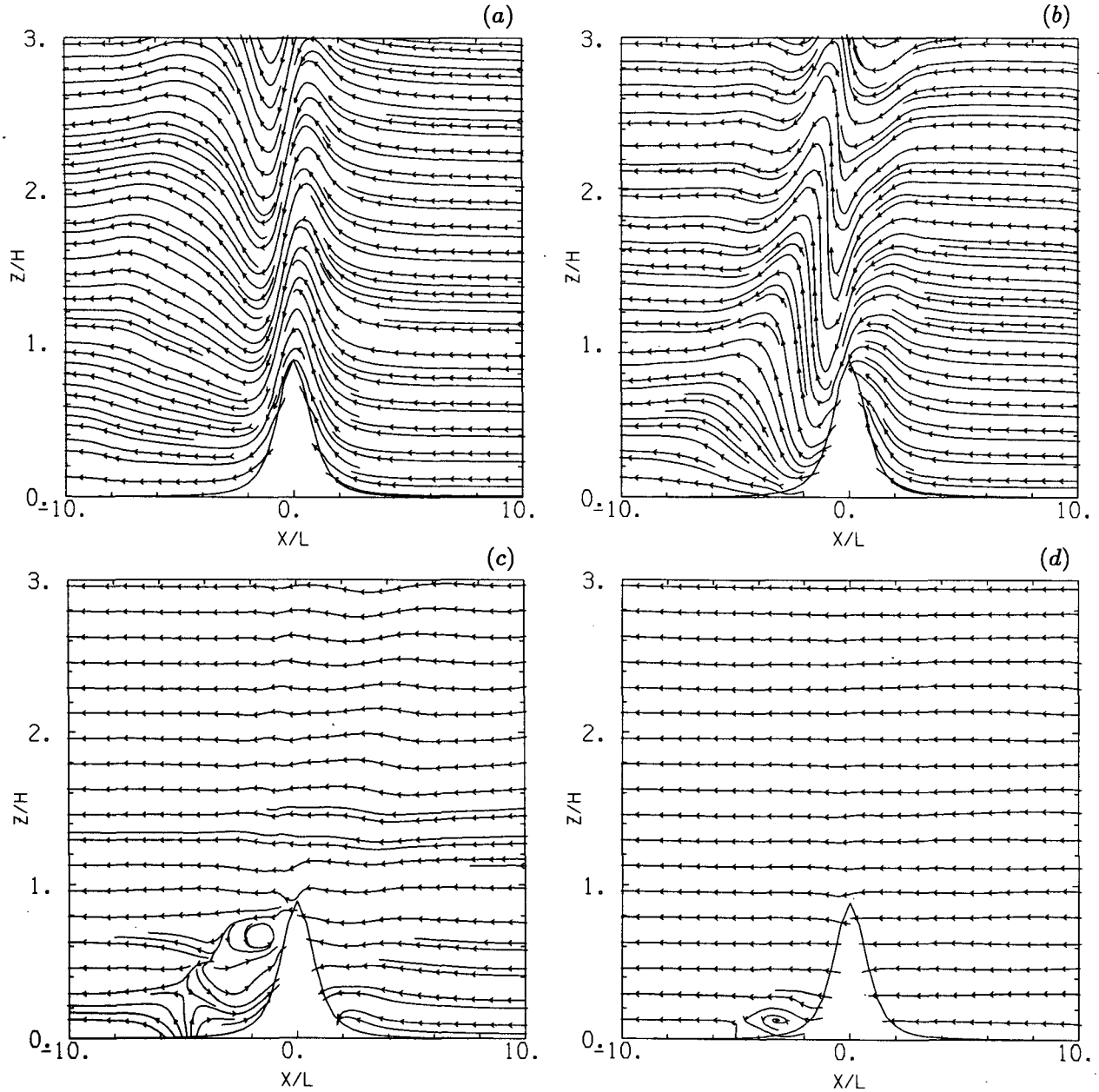

FIG. 3. Steady-state streamlines in vertical cross section through the center plane for Fr = (a) 2.2, (b) 0.66, (c) 0.22, and (d) 0.055.

sured by the maximum value of the nondimensional horizontal velocity in the reversed flow in the lee of the obstacle as a function of Fr. Figure 5b shows the depth of the lee vortices as measured by the height (normalized by h) of the reversed flow in the lee of the obstacle as a function of Fr. Both curves exhibit a similar dependence on Fr. These two features remain aproximately constant within the range Fr $\sim$ 0.2–0.4 and decrease rapidly both when Fr $\rightarrow$ 0 or Fr $\rightarrow$ 0.5. This result is reasonable inasmuch as in the limit Fr $\rightarrow$ 0 the solution should approach two-dimensional potential flow, while in the limit Fr $\rightarrow \infty$ the solution should approach three-dimensional potential flow; in both limits the vortices should disappear. Figure 5c displays the width of the vortex couplet in the spanwise direction measured by the maximum distance between closed surface streamlines; the shrinking of the vortices with increasing Fr is apparent. Finally, Fig. 5d shows the distance of the vortices from the center of the obstacle measured by the distance of the position of the maximal reversed flow in the lee from the center of the obstacle; as Fr increases the lee vortices approach the

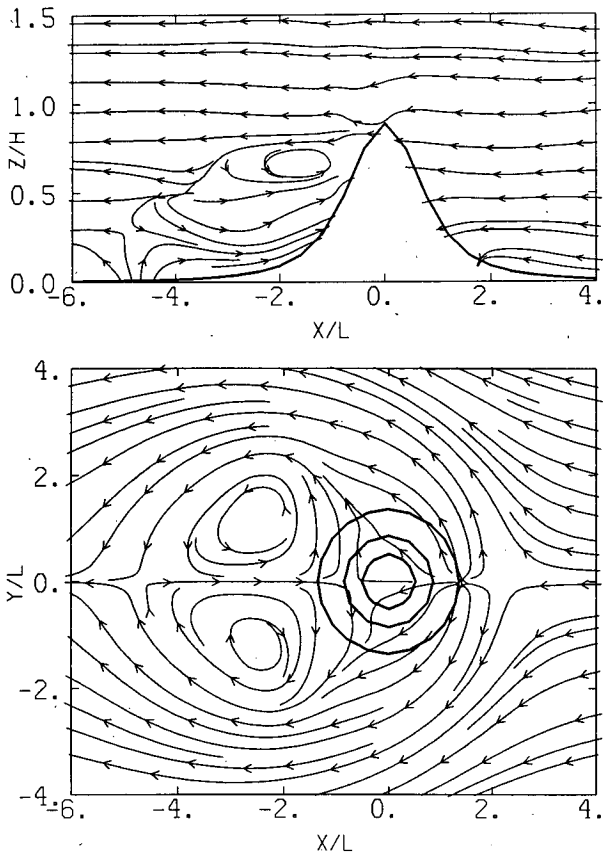

FIG. 4. Close-up view of the flow pattern in vertical cross section on the center plane and the surface for the experiment with Fr = 0.22, for comparison with a similar sketch of the laboratory experiment of Hunt and Snyder (1980, see their Fig. 15a).

obstacle. We include the point at Fr = 0.55 in Fig. 5 even though no well-formed vortex appeared because it is indicative of the incipient formation of a stagnation point at the surface. While one could measure the intensity and depth of the reversed flow, the estimation of the width and distance from the obstacle of the "vortex" was more subjective.

The results shown in Figs. 5 are in qualitative agreement with the laboratory experiments of HS. Their Fig. 15a–e contains sketches of the flows for Fr = 0.2, 0.4, 1.0, 1.7 and ∞. Comparing their flow at Fr = 0.2, with their flow at Fr = 0.4, one observes that the lee vortices are positioned approximately twice as near to the obstacle center (cf. Fig. 5d) and are about half the size (cf. Fig. 5c). The depth of their vortices decreases slightly from Fr = 0.2 to 0.4 but, in both cases, not very far from the nearly constant value obtained in this range of Fr shown in Fig. 5b. In HS's Fig. 15c (Fr = 1.0), there is only a very small region of reversed flow in the lee, and in our simulations, there are no lee vortices above Fr $\approx$ 0.55. This suggests to us that the lee vortices found at Fr = 0.2 and 0.4 in HS are similar to the ones simulated herein as both exist for Fr = 0.2 and 0.4, both virtually disappear at Fr = 1.0, and both exhibit similar characteristics.

The HS Fig. 15d–e shows that the small region of reversed flow observed at Fr = 1.0 enlarges when Fr = 1.7 and ∞. We believe this reappearance of a large region of reversed flow is a manifestation of a three-dimensional, separated boundary layer. At the other extreme, Brighton's (1978) experiments exhibit lee-vortex formation for very low Fr($\leq$0.1); it is argued therein that these vortices are the result of boundary-layer separation restricted to horizontal planes by the strong stratification. We believe the present numerical experiments provide an important complement to the laboratory studies as those features not exclusively dependent on boundary-layer separation may be isolated. For Fr outside the range 0.1–0.5, the present study supports the notion that boundary-layer separation is responsible for the lee vortices, since without a boundary layer, no lee vortices form in this range. However, within this range of Fr, the present study suggests there is a coexisting, likely dominant, mechanism at work.

Before leaving this section, we report that the lee vortices in our simulations showed no inclination to shed from the obstacle, even after we perturbed them. However, Smolarkiewicz et al. (1988) found shedding vortices in simulations of flow past Hawaii even though the vortices were produced without a boundary layer present. We believe that it is the asymmetry of the mountain shape that induces shedding in those experiments; we have performed simulations of flow past an elliptical obstacle with minor axis turned at a slight angle to the mean wind and simulated shedding. Since vortex shedding is complicated enough to warrant a separate study and since our preliminary results just scratch the surface, we think it premature to discuss these findings in detail herein.

4. The lee vortices

a. Simulation of lee vortices

The lee vortices have been explained in terms similar to those used in describing the formation of vortices in the wake of a cylinder in a homogeneous flow. That explanation is that the viscous boundary layer on the cylinder suffers an adverse pressure gradient as it passes toward the rear and so it separates; the resulting flow carries its vorticity far from the cylinder (Batchelor 1967, pp. 325–331). In explaining the lee vortices in the case at hand, the stratification is presumed to act as a constraint that forces fluid to remain in horizontal planes thus rendering the problem similar to that of the cylinder (Brighton 1978). This argument cannot possibly account for the lee vortices in our case, however, since our free-slip boundary conditions do not produce a frictional boundary layer and so there is no frictionally produced vertical vorticity at the obstacle.

One might wonder whether the separation is an artifact of the finite-difference approximation to the gov-

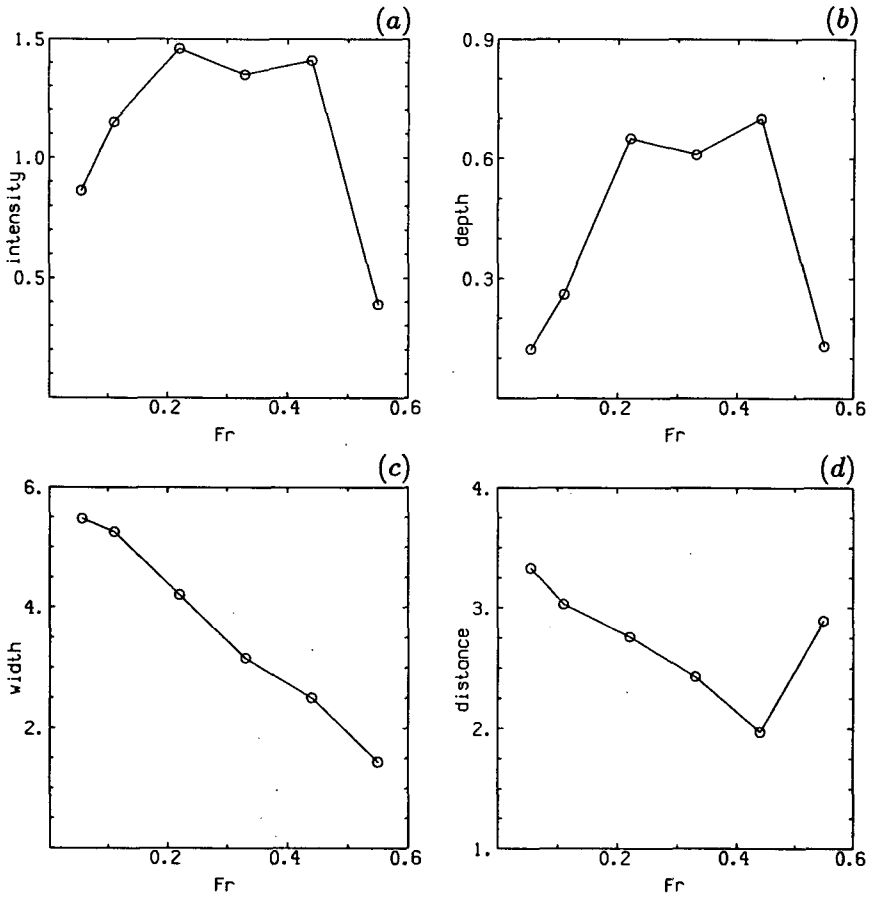

FIG. 5. Characteristics of the lee vortices vs Froude number: (a) intensity; (b) depth; (c) width; (d) distance from the center of the hill.

erning equations and boundary conditions. At the time the simulation is displayed in Fig. 4 that experiment was restarted with zero stratification. After an additional 21 time units (the time required for fluid to advect through the domain), the three-dimensional potential-flow solution was established and maintained by the model, as expected from elementary fluid dynamics. Therefore, the vortices are not produced by a spurious source at the surface and are intimately related to the stratification.

The only possible source of vertical vorticity in the present experiments is the tilting of horizontal vorticity in the lee of the obstacle. As the assumed wind upstream is constant, there is no ambient horizontal vorticity and so the requisite horizontal vorticity must be produced by the baroclinicity associated with isentropic surfaces bending upward and downward as the flow passes over and round the obstacle. As mentioned in the previous section, linear theory is formally invalid at the Fr for which the vortices appear; however, linear theory and its higher-order correction have much to say about the physics of the lee vortices.

b. Linear analysis and its next-order correction

Consider the steady, inviscid hydrostatic[1] equations linearized about a constant wind in the x direction u_0:

$$u_0 \frac{\partial u_1}{\partial x} = -\frac{\partial \phi_1}{\partial x} \tag{2}$$

$$u_0 \frac{\partial v_1}{\partial x} = -\frac{\partial \phi_1}{\partial y} \tag{3}$$

$$\frac{\partial \phi_1}{\partial z} = b_1 \tag{4}$$

$$u_0 \frac{\partial b_1}{\partial x} = -N^2 w_1 \tag{5}$$

$$\frac{\partial u_1}{\partial x} + \frac{\partial v_1}{\partial y} + \frac{\partial w_1}{\partial z} = 0 \tag{6}$$

[1] We have conducted an experiment at Fr = 0.33 with a hydrostatic version of Clark's model and found that the flow features discussed in this paper are unrelated to nonhydrostatic effects.

where now $N^2 \equiv \partial b_0/\partial z$ and the other symbols have their usual meaning. Along with (2)–(6) we have the relation

$$w_1 = u_0 \frac{\partial \delta_1}{\partial x} \tag{7}$$

where δ_1 is the perturbation displacement field. Finally, Eqs. (5) and (7) lead to

$$b_1 = -N^2 \delta_1. \tag{8}$$

The cross derivatives of (2) and (3), together with the condition at infinity, $\zeta_1 = 0$, inform us that the perturbation vertical vorticity $\zeta_1 = 0$ for all (x, y). Hence the vertical vorticity we seek must enter at a higher order (in the amplitude expansion from which linear theory emerges at first order). It is easy to show that at the next order of approximation the vertical vorticity equation is

$$u_0 \frac{\partial \zeta_2}{\partial x} = \xi_1 \frac{\partial w_1}{\partial x} + \eta_1 \frac{\partial w_1}{\partial y} \tag{9}$$

where $\xi_1 \equiv -\partial v_1/\partial z$ and $\eta_1 \equiv \partial u_1/\partial z$ are respectively the x and y components of vorticity at first order. Equation (9) says that vertical vorticity is created at second order by the tilting of first-order horizontal vorticity by the first-order vertical velocity. Equations for ξ_1 and η_1 can be derived from (2)–(4):

$$u_0 \frac{\partial \xi_1}{\partial x} = \frac{\partial b_1}{\partial y}; \quad u_0 \frac{\partial \eta_1}{\partial x} = -\frac{\partial b_1}{\partial x}. \tag{10a, b}$$

Equations (10a, b) remind us that ξ_1 and η_1 are generated through baroclinicity. Using (7), (8) and $\xi_1 = \eta_1 = 0$ at $x = \infty$ (assuming flow from right to left, $u_0 < 0$), one can show further that

$$\xi_1 = \frac{N^2}{u_0} \int_x^\infty \frac{\partial \delta_1}{\partial y}\, dx; \quad \eta_1 = \frac{N^2}{u_0} \delta_1. \tag{11a, b}$$

Within the confines of linear theory, $\delta_1 \approx$ the height of the topography close to the lower surface. Thus for a mean flow from right to left, $\eta_1 < 0$ and mirrors the topography. However $\xi_1 < 0$ for $y < 0$ and $\xi_1 > 0$ for $y > 0$ and trails indefinitely downstream from the obstacle. We display a schematic diagram of the vortex lines in Fig. 6a. The interpretation is, therefore, that the baroclinically produced vorticity in the y direction as the air ascends is exactly cancelled as it descends on the lee slope. However, vorticity produced in the x direction never encounters any cancelling effect and is simply swept downstream. [This is consistent with Smith's (1980) finding of a permanent lateral deflection of the surface streamlines downwind of the obstacle.] Given this fore–aft asymmetry in the ξ field it is easy to see that (9) implies negative (positive) vertical vorticity on the lee slope for $y < 0$ ($y > 0$). Above the lower surface δ_1 no longer mirrors the topography but according to Smith's (1980) solution (his Fig. 5) δ_1 has

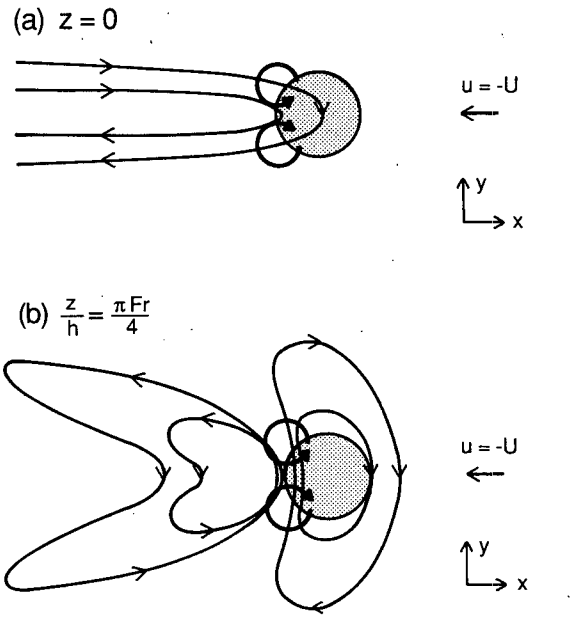

FIG. 6. Vortex lines as deduced from linear theory along with an indication of the sense of the vertical vorticity inferred from the next-higher-order correction to the linear theory at (a) the lower surface and (b) 1/8 of a vertical wavelength aloft.

an upwind phase shift of the upward displacement and downward displacement ($\delta_1 < 0$) in the lee which gradually approaches zero with downstream distance. This distribution of δ_1 allows one to infer from (11a, b) a vortex-line system as depicted in Fig. 6b (based on our inference from Smith's Fig. 1b). Since δ_1 and $\partial \delta_1/\partial y$ change sign in the lee of the hill a double-structured system is implied.

We can go one step further with (9); substituting for w_1 in (9) from (5) we can show that

$$\zeta_2 = -\frac{1}{N^2}\left(\xi_1 \frac{\partial b_1}{\partial x} + \eta_1 \frac{\partial b_1}{\partial y}\right). \tag{12}$$

Using (8) in (12), we obtain

$$\zeta_2 = \xi_1 \frac{\partial \delta_1}{\partial x} + \eta_1 \frac{\partial \delta_1}{\partial y}. \tag{13}$$

With (13) and our discussion of ξ_1, η_1 and δ_1 it is a straightforward matter to sketch the sense of ζ_2 as we did in Figs. 6a–b. Equation (12) may be alternatively derived by considering that the "potential vorticity" of the system before linearization $\omega \cdot \nabla b = 0$ (where ω is the vorticity vector) upstream and, by Ertel's theorem (e.g., see Dutton 1976, p. 381), must be so throughout the domain. Thus

$$\omega \cdot \nabla b = \zeta_2 N^2 + \xi_1 \frac{\partial b_1}{\partial x} + \eta_1 \frac{\partial b_1}{\partial y} + O(\epsilon^3) = 0 \tag{14}$$

where ϵ is an amplitude-measuring parameter.

c. Analysis using Ertel's theorem

The foregoing analysis suggests that we should exploit Ertel's theorem in analyzing our fully nonlinear model results as it is generally applicable. Ertel's theorem is that for an inviscid adiabatic fluid the "potential vorticity" is conserved:

$$\frac{d}{dt}\left(\frac{1}{\bar{\rho}}\,\omega\cdot\nabla\Theta\right)=0, \tag{15}$$

where $\bar{\rho}$ is the height-dependent density of the base state (e.g., see Rotunno and Klemp 1985), and Θ is the potential temperature. In our initial state $\omega\cdot\nabla\Theta = 0$ for all x, and by (15), it must remain so for all t, i.e.,

$$\omega\cdot\nabla\Theta=0. \tag{16}$$

The geometrical interpretation of (16) is that vortex lines must lie in a surface of constant Θ. Moreover, if the flow is steady, the trajectories, which also remain on isentropic surfaces, are identical to streamlines, and then the cumbersome problem of displaying a complex three-dimensional flow may be reduced to the simpler two-dimensional analysis of flow on isentropic surfaces.

The accuracy with which the Ertel theorem is satisfied in the model has been evaluated considering the field of error defined as

$$\mathrm{ER}|_{\Theta=\mathrm{const}}=\frac{2}{\pi}\cos^{-1}\left(\frac{\omega\cdot\nabla\Theta}{\|\omega\|\cdot\|\nabla\Theta\|}\right)-1. \tag{17}$$

In all cases discussed in this paper the mean value of ER was a few percent with standard deviation an order of magnitude smaller. The extreme values were, however, large but confined to the regions where the Θ surfaces lowered to the point of intersecting the lower boundary of the model; consequently their gradients could not be accurately determined. Apart from this special situation, ER was generally negligible, indicating that the source of error was primarily in the evaluation of ER.

Figure 7 shows the vortex lines on the isentropic surface originating upstream at $z/h = \pi\,\mathrm{Fr}/2$ for the experiment shown in Fig. 4 (Fr = 0.22). The solid and dashed lines represent positive and negative displacements, respectively, of the isentrope. The large hole seen in the center is due to the intersection of the isentrope with the hill. It is apparent that the entire system of vortex lines is divided into two separate structures as we had inferred from the linear theory. In the linear model *vorticity vectors are tangent to isentropic surfaces of the horizontally homogeneous base state* (the linear version of Ertel's theorem) and so there is no generation of vertical vorticity. The essential difference between the linear and nonlinear solution is not so much in the geometry of isentropic surfaces but rather in the release of the linear vorticity constraint which allows for vortex lines to follow the *actual* isentropes

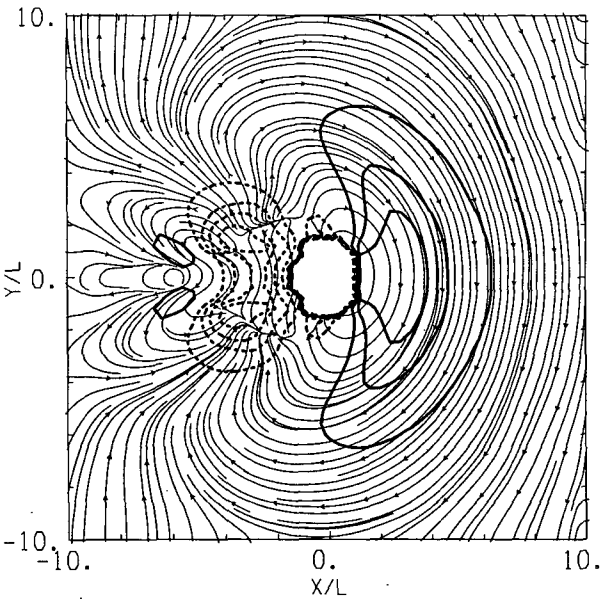

FIG. 7. Vortex lines on the isentropic surface of undisturbed height, $z/h = \pi\,\mathrm{Fr}/2$ for the experiment with Fr = 0.22. The contour lines show the displacement field of the isentrope (contour lines are plotted for the values, 8⅓, 6⅔, 5, 3⅓, −3⅓, −6⅔, −10, $-13\frac{1}{3}\times10^{-5}\,h$).

(instead of the those of the base state). It is apparent from Fig. 7 that the strongest tilting of vortex lines toward the vertical occurs in the lee of the hill where vortex lines cross lines of constant displacement at the steep slopes of the Θ surface. At the upwind-side vortex lines remain parallel to the lines of constant displacement and this indicates zero vertical vorticity.

5. Discussion

The flow of a uniformly stratified fluid past a three-dimensional obstacle becomes highly complex as the Froude number passes below unity. In this regime linear theory fails (since it requires a large Froude number for its validity), as does potential-flow-type theories (which require an extremely small Froude number for their validity). The present numerical experiments were conceived as a means to bridge the gap between these two approaches. Our calculations were carried out using a free-slip condition between the fluid and the lower bounding surface in order to isolate the purely inviscid aspects of the stratified fluid flow from those due to the viscous boundary layer. We found that as the Froude number passed below a critical value (~0.5) vertically oriented vortices on the lee side, and a zone of flow reversal on the windward side, appear.

The mechanism for generation of the vertically oriented vorticity of the lee vortices is through the tilting of the horizontally oriented vorticity, but since there is no such horizontally oriented vorticity in the base state, it must be generated through baroclinic production as the isentropes bend upward, and subsequently

downward, as the flow passes over the obstacle. The shape of the isentropic surfaces is thus crucial for understanding the vorticity distribution. Linear gravity-wave theory gives a good qualitative description of the shape of the isentropes but predicts zero vertical vorticity. By carrying out the amplitude expansion, from which linear theory emerges at first order, to the next order, we find that the vertical vorticity is given by the tilting of the first-order baroclinically produced horizontal vorticity by the first-order vertical velocity. We show that these deductions may be made from Ertel's theorem and proceed to analyze the fully nonlinear model results in the framework supplied by the conservation of potential vorticity.

Although the linear theory gives a good qualitative description of the form of the solution, it seems far less useful when it comes to understanding the transition we observe as Fr $\searrow$ 0.5. Certainly the most important thing that happens at Fr $\searrow$ 0.5 is the appearance of inchoate stagnation points. Although it is technically invalid, Smith (1980) shows that the linear solution implies flow stagnation at the lower surface on the windward side at Fr $\approx$ 0.4. The relevance of this prediction will be evaluated in Part II of this study as we then concentrate on the windward-side flow. However, on the leeward side the linear solution (which is invalid since the isentropes collapse and intersect the lower surface there when Fr $\approx$ 2) gives no suggestion of decelerated flow. This and our deduction that a vortex pair, with implied reversed flow on the center axis, emerges in the next-order correction to linear theory leads us to the conclusion that the prediction of the leeward stagnation point is beyond the reach of linear theory. Although the second-order theory suggests reversed flow on the lee side, an analytical prediction of the appearance of flow stagnation on the leeward side as Fr $\searrow$ 0.5 has thus far eluded us.

Our comparison of the present results with laboratory experiments suggests there is more than one mechanism producing lee vortices. For Fr $>$ 0.5 and Fr very small, the contention that lee vortices are produced by boundary-layer separation is supported by the present calculations as we deliberately eliminate a boundary layer and no vortices occur in this range of Fr. However, within the range $0.1 \leqslant \text{Fr} \leqslant 0.5$ (which covers most circumstances of flow past mesoscale mountains), the present study indicates that the purely inviscid mechanism described herein may coexist with, and likely dominate, that of boundary-layer separation.

Several observational tests of the present mechanism immediately suggest themselves. First, and most obviously, the lee vortices should have deep warm cores. Casual observation of cloud photographs show the absence of clouds directly in the lee of Hawaii; it would be fairly simple to investigate whether the absence of clouds there is a manifestation of a pair of warm-core vortices. Second, the horizontally averaged absolute magnitude of vertical vorticity ought to decrease gradually ($\sim z^{-1}$) over the depth of the fluid for the baroclinic vortices, while, in contrast, the same quantity associated with frictionally produced vortices ought to decrease abruptly above the summit. We also believe that field verification of the properties of the simulated lee vortices indicated in Fig. 5 should be relatively straightforward.

REFERENCES

Arakawa, A., 1966: Computational design for long term integration of the equations of motion: Two-dimensional incompressible flow. Part 1. *J. Comput. Phys.*, **1**, 119–143.

Batchelor, G. K., 1967: *An Introduction to Fluid Dynamics.* Cambridge University Press, 615 pp.

Brighton, P. W., 1978: Strongly stratified flow past three-dimensional obstacles. *Quart. J. Roy. Meteor. Soc.*, **104**, 289–307.

Castro, I. P., W. H. Snyder and G. L. Marsh, 1983: Stratified flow over three-dimensional ridges. *J. Fluid Mech.*, **135**, 261–282.

Clark, T. L., 1977: A small scale dynamic model using a terrain-following coordinate transformation. *J. Comput. Phys.*, **24**, 186–215.

——, and Farley, 1984: Severe downslope windstorm calculations in two and three spatial dimensions using anelastic interactive grid nesting: A possible mechanism for gustiness. *J. Atmos. Sci.*, **41**, 329–350.

Crapper, G. D., 1959: A three-dimensional solution for waves in the lee of mountains. *J. Fluid Mech.*, **6**, 51–76.

Drazin, P. G., 1961: On the steady flow of a fluid of variable density past an obstacle. *Tellus*, **13**, 239–251.

Dutton, J. A., 1976: *The Ceaseless Wind.* McGraw-Hill, 579 pp.

Hawthorne, W. R., and M. E. Martin, 1955: The effect of density gradient and shear on the flow over a hemisphere. *Proc. Roy. Soc. London*, **A232**, 184–195.

Hunt, C. R., and W. H. Snyder, 1980: Experiments on stably and neutrally stratified flow over a model three-dimensional hill. *J. Fluid Mech.*, **96**, 671–704.

Lilly, D. K., 1965: On the computational stability of numerical solutions of time-dependent non-linear geophysical fluid dynamics problems. *Mon. Wea. Rev.*, **93**, 11–26.

Long, R. R., 1953: Some aspects of the flow of stratified fluids. I. A theoretical investigation. *Tellus*, **5**, 42–48.

Pierrehumbert, R. T., and B. Wyman, 1985: Upstream effects of mesoscale mountains. *J. Atmos. Sci.*, **42**, 977–1003.

Queney, P., 1948: The problem of air flow over mountains: A summary of theoretical studies. *Bull. Amer. Meteor. Soc.*, **29**, 16–26.

Rotunno, R., and J. B. Klemp, 1985: On the rotation and propagation of simulated supercell thunderstorms. *J. Atmos. Sci.*, **42**, 271–292.

Smith, R. B., 1977: The steepening of hydrostatic mountain waves. *J. Atmos. Sci.*, **34**, 1634–1654.

——, 1980: Linear theory of stratified hydrostatic flow past an isolated mountain. *Tellus*, **32**, 348–364.

Smolarkiewicz, P. K., 1984: A fully multidimensional positive definite advection transport algorithm with small implicit diffusion. *J. Comput. Phys.*, **54**, 325–362.

——, and T. L. Clark, 1986: The multidimensional positive definite advection transport algorithm: Further development and applications. *J. Comput. Phys.*, **67**, 396–438.

——, R. Rasmussen and T. L. Clark, 1988: On the dynamics of Hawaiian cloud bands: Island forcing. *J. Atmos. Sci.*, **45**, 1872–1905.

Snyder, W. H., R. S. Thompson, R. E. Eskridge, R. E. Lawson, I. P. Castro, J. T. Lee, J. C. R. Hunt and Y. Ogawa, 1985: The structure of strongly stratified flow over hills: Dividing streamline concept. *J. Fluid Mech.*, **152**, 249–288.